Int. J. Solids Structures, 1974, 10, pp. 243–260. Pergamon Press. Printed in Gt. Britain.

THE DYNAMIC RESPONSES OF CYLINDRICAL SHELLS INCLUDING GEOMETRIC AND MATERIAL NONLINEARITIES*

RICHARD W.-H. WU† and EMMETT A. WITMER‡
Massachusetts Institute of Technology, Cambridge, Massachusetts 02139

(*Received* 29 *May* 1973; *revised* 2 *August* 1973.)

Abstract—The methods of finite-element analysis are applied to the problem of large deflection elastic–plastic dynamic responses of cylindrical shells to transient loading. Assumed-displacement quadrilateral finite-elements of a cylindrical panel are used to idealize the cylindrical shell structure. The formulation is based upon the Principle of Virtual Work and D'Alembert's Principle. A direct numerical integration procedure is employed to solve the resulting equations of motion timewise. The present predicted dynamic responses of an explosively-loaded clamped cylindrical panel are compared with other independent predictions and with experimentally measured responses; very good agreement is observed.

1. INTRODUCTION

Various flight, water, and land vehicles and stationary structures may be subjected to collision, impact, blast, and/or other intensive transient loads which can cause large transient structural deformation and damage. The need for accurate and efficient methods for structural analysis and design, especially for this category of large-deflection (geometrically nonlinear) and elastic–plastic (materially nonlinear) dynamic response problems has been increasingly evident recently.

Various methods of analysis have been devised for predicting this kind of response behavior. Among them the two most general and versatile methods are the finite-difference method and the finite-element method. In the finite-difference method, the space and time derivatives of the field variables in the governing differential equations or in the variational (energy) functional are replaced by appropriate finite-difference expressions. As for the finite-element method which is most systematically based on variational principles, the entire domain of the structure is idealized as an assemblage of a finite number of regions (elements) which are connected at a finite number of nodes along inter-region boundaries, and suitable interpolation functions are selected to describe the distribution of each quantity throughout each finite element. The resulting system of second-order ordinary differential equations of motion are solved timewise by using an appropriate integration operator. The relative ease and versatility with which the finite-element method can be applied to structures with complicated geometric shape, material properties, and boundary conditions in comparison with the finite-difference method is often regarded as an important attribute of the finite-element method.

* This work was supported by the Army Materials and Mechanics Research Center under Contract DAAG46-72-C-0212; Dr. J. Adachi was the technical monitor.
† Senior Research Engineer, Aeroelastic and Structures Research Laboratory.
‡ Professor of Aeronautics and Astronautics.

For analyzing the problems of the present category—large deflection, elastic–plastic dynamic responses, the finite-difference method has undergone intensive development and has been applied, for example, to beams, rings, plates, and single-layer shells[1–6]. More recently, it has been extended to analyzing multi-layer shells[7] and soft-bonded layered shells[8]. However, only limited finite-element development has been reported for this class of problems[9–12]. In this paper, application of the finite-element method is extended to cylindrical shells undergoing large-deflection elastic–plastic responses.

The conventional form of the finite-element formulation is presented here in general three-dimensional tensor form. This is then specialized to represent a cylindrical shell structure which is idealized as an assemblage of a finite number of quadrilateral cylindrical panel elements. Comparisons of the present predictions with other independent predictions and with experiments for an explosively loaded cylindrical panel are made.

2. GENERAL FORMULATION

2.1 *The spatial finite-element approximation*

Consider a deformed continuum in equilibrium. The Principle of Virtual Work states that the virtual work, δW, done by the external forces (body forces and surface tractions) is equal to the virtual work, δU, of the internal stresses, i.e.

$$\delta U - \delta W = 0 \tag{1}$$

where

$$\delta U = \int_V S^{ij}\,\delta\gamma_{ij}\,\mathrm{d}V \tag{1a}$$†

$$\delta W = \int_V \rho B^i\,\delta u_i\,\mathrm{d}V + \int_{A\sigma} T^i\,\delta u_i\,\mathrm{d}A. \tag{1b}$$

In this equation S^{ij} is the Kirchhoff stress tensor, B^i is the body force, T^i is the externally-applied surface tractions, γ_{ij} is the Lagrangian strain tensor, u_i is the displacement components, ρ is the mass density, and only displacement variations (δ) are permitted. All pertinent quantities are described consistently with respect to a curvilinear coordinate system (termed Lagrangian coordinates) ξ^i. Also, the integrations extended over the entire undeformed volume, V, of the continuum which is bounded by the undeformed surface A. The surface A may be divided into a prescribed-surface-traction boundary, A_σ, and a prescribed-displacement boundary A_u.

By employing the concept of D'Alembert's Principle, the body forces ρB^i may be regarded as consisting of D'Alembert inertia forces ($-\rho\ddot{u}^i$) and other body forces ρf^i (gravitational, magnetic, etc.). Thus,

$$\rho B^i = -\rho\ddot{u}^i + \rho f^i \tag{2}$$

where ($\dot{}$) denotes partial differentiation with respect to time t.

The nonlinear strain–displacement relation may be expressed as

$$\gamma_{ij} = (u_{i,j} + u_{j,i} + u_{a,i}u^a_{,j})/2 \tag{3}$$

† The customary tensor indicial and summation convention are used. Latin minuscules range over the values 1, 2, and 3.

where $(\ )_{,i}$ denotes covariant differentiation with respect to ξ^i using the metric tensors of the undeformed state.

Let the continuum be subdivided conceptually into N finite elements. Then, one may write equation (1) as the sum of the contributions from each of the finite elements as follows:

$$\sum_{n=1}^{N} (\delta U_n - \delta W_n) = 0 \tag{4}$$

where

$$\delta U_n = \int_{V_n} S^{ij}\, \delta\gamma_{ij}\, \mathrm{d}V \tag{4a}$$

$$\delta W_n = \int_{V_n} \rho(-\ddot{u}^i + f^i)\, \delta u_i\, \mathrm{d}V + \int_{A_n} T^i\, \delta u_i\, \mathrm{d}A \tag{4b}$$

where V_n is the volume of the nth discrete element, and A_n is the portion of the surface area of element n, over which the surface traction T^i is prescribed.

If one chooses for each element an assumed displacement field of the form

$$u_i(\xi^j, t) = \lfloor N_i(\xi^j)\rfloor\{q(t)\} \tag{5}$$

where $N_i(\xi^j)$ is an appropriately assumed interpolation function and $\{q\}$ represents conveniently chosen generalized nodal displacements of the element, it follows that

$$\delta u_i = \lfloor N_i\rfloor\{\delta q\}. \tag{6}$$

Hence,

$$\delta\gamma_{ij} = \lfloor D_{ij}\rfloor\{\delta q\} + \lfloor q\rfloor\{D_{ai}\}\lfloor D_j{}^a\rfloor\{\delta q\} \tag{7}$$

where D_{ij}, D_{ai}, and $D_j{}^a$ are the appropriate associated differential operators which may be expressed symbolically in the form

$$\begin{aligned} &\lfloor D_{ij}\rfloor = \lfloor N_{i,j} + N_{j,i}\rfloor/2 \\ &\lfloor D_{ai}\rfloor = \lfloor N_{a,i}\rfloor, \qquad \lfloor D_j{}^a\rfloor = \lfloor N_{,j}{}^a\rfloor. \end{aligned} \tag{7a}$$

Employing equations (6) and (7), equation (4) becomes

$$\sum_{n=1}^{N} \lfloor\delta q\rfloor\Big(\int_{V_n} \{D_{ij}\}S^{ij}\, \mathrm{d}V + \int_{V_n} \{D_{ai}\}\lfloor D_j{}^a\rfloor S^{ij}\, dV\{q\} - \int_{V_n} \{N_i\}\rho f^i\, \mathrm{d}V - \int_{A_n} \{N_i\}_b T^i\, \mathrm{d}A + \int_{V_n} \{N_i\}\rho\lfloor N^i\rfloor\, \mathrm{d}V\{\ddot{q}\}\Big) = 0 \tag{8}$$

where subscript "b" is used to signify that $\{N_i\}$ are evaluated along the element boundary.

One next proceeds to express the stresses in terms of the displacements via the stress–strain relations and the strain–displacement relation, as follows:

$$S^{ij} = E^{ijkl}(\lfloor D_{kl}\rfloor\{q\} + \lfloor q\rfloor\{D_{ck}\}\lfloor D_l{}^c\rfloor\{q\}/2 - \gamma_{kl}{}^p) \tag{9}$$

where E^{ijkl} consists of elastic constants and $\gamma_{kl}{}^p$ represents the component of the total plastic strain (or other given initial strain). Substituting equation (9) into equation (8), also since the element nodal generalized displacements $\{q\}$ for different elements are not completely independent, a transformation $[J]$ is required to relate the element nodal displacements to

independent global nodal generalized displacements $\{q^*\}$ for the discrete-element assemblage, one obtains:

$$\sum_{n=1}^{N} [\delta q^*]([m]\{\ddot{q}^*\} + [k]\{q^*\} - \{f\} - \{f_q^{NL}\} - \{f_p^{L}\} - \{f_p^{NL}\}) = 0 \tag{10}$$

where

$$[m] = [J]^T \int_{V_n} \{N_i\}\rho[N^i]\, dV[J]$$

$$[k] = [J]^T \int_{V_n} \{D_{ij}\}E^{ijkl}[D_{kl}]\, dV[J]$$

$$\{f\} = [J]^T \left(\int_{V_n} \rho\{N_i\}f^i\, dV + \int_{A_n} \{N_i\}_b T^i\, dA \right)$$

$$\{f_q^{NL}\} = [J]^T \Bigg(- \int_{V_n} \{D_{ij}\}E^{ijkl}\langle [q]\{D_{ck}\}[D_l^c]\{q\}/2\rangle\, dV$$

$$- \int_{V_n} \{D_{ai}\}[D_j^a]E^{ijkl}\langle [D_{kl}]\{q\} + [q]\{D_{ck}\}[D_l^c]\{q\}/2\rangle\, dV\{q\}) \Bigg)$$

$$\{f_p^{L}\} = [J]^T \int_{V_n} \{D_{ij}\}E^{ijkl}\gamma_{kl}{}^p\, dV$$

$$\{f_p^{NL}\} = [J]^T \int_{V_n} \{D_{ai}\}[D_j^a]E^{ijkl}\gamma_{kl}{}^p\, dV\{q\} \tag{10a}$$

performing the summation and because the variation $\{\delta q^*\}$ can be independent and arbitrary, the following equilibrium equation is obtained[10, 11, 13]:

$$[M]\{\ddot{q}^*\} + [K]\{q^*\} = \{F\} + \{F_q^{NL}\} + \{F_p^{L}\} + \{F_p^{NL}\} \tag{11}$$

where $[M]$ and $[K]$ are the usual global mass and stiffness matrix, respectively (for linear-elastic small deflection behavior), $\{F_q^{NL}\}$ represents a "generalized loads" vector arising from large deflections, $\{F_p^{L}\}$ and $\{F_p^{NL}\}$ are the generalized load vectors due to the presence of plastic strains and are associated, respectively, with the linear and nonlinear terms of the strain–displacement relations.

It perhaps should be noted that by solving equation (8) directly, an alternate formulation wherein the stresses are retained in explicit form has been presented in [9] and [10].

2.2 *Timewise solution process*

Given a set of initial conditions $\{q^*\}$ and $\{\dot{q}^*\}$ at $t = 0$, $\{F\}$ as a function of time, and the proper boundary conditions, equation (11) may be solved by employing an appropriate timewise finite-difference operator. In the present analysis, the Houbolt (4-point backward difference) operator is chosen for use. The $\{\ddot{q}^*\}$ at any instant of time t_{m+1} is approximated by

$$\{\ddot{q}^*\}_{m+1} = (2\{q^*\}_{m+1} - 5\{q^*\}_m + 4\{q^*\}_{m-1} - \{q^*\}_{m-2})/(\Delta t)^2. \tag{12}$$

Employing equation 12, equation 11 becomes

$$(2[M] + (\Delta t)^2[K])\{q^*\}_{m+1} = [M](5\{q^*\}_m - 4\{q^*\}_{m-1} + \{q^*\}_{m-2}) + (\Delta t)^2(\{F\}_{m+1} + \{F_q^{NL}\}_{m+1} + \{F_p^{L}\}_{m+1} + \{F_p^{NL}\}_{m+1}). \tag{13}$$

This calculation method is not self-starting; a special "commencing sequence"[14] which provides $\{q^*\}_1$ at $t_1 = \Delta t$ and $\{q^*\}_{-1}$ at a negative (fictitious) time $t_{-1} = -\Delta t$ can be used.

It perhaps should be noted that in equation (13), the generalized nodal load vectors $\{F_q^{NL}\}_{m+1}$, $\{F_p^{L}\}_{m+1}$, and $\{F_p^{NL}\}_{m+1}$ which may be due to large deflections and/or elastic–plastic effects depend on the displacements (or stresses, strains) at that time instant t_{m+1}, but this information remains to be determined. Thus, extrapolation (or iteration) is needed at each time step of calculation. Linear extrapolation from known information at t_m and t_{m-1} is employed in the present calculations to estimate these force values, i.e.

$$(\{F_q^{NL}\} + \{F_p^{L}\} + \{F_p^{NL}\})_{m+1} \doteq 2(\{F_q^{NL}\} + \{F_p^{L}\} + \{F_p^{NL}\})_m - (\{F_q^{NL}\} + \{E_p^{L}\} + \{F_p^{NL}\})_{m-1}. \quad (14)$$

Also, it is seen that the evaluation of $\{F_q^{NL}\}$, $\{F_p^{L}\}$ and $\{F_p^{NL}\}$ as in equation (11) involves volume integration over each discrete element of certain quantities which change with time and hence must be re-evaluated, in general, at each instant of time. For the structure undergoing large deflection, elastic–plastic behavior, it is impractical to evaluate these volume integrals analytically. Accordingly, numerical integration such as Gaussian quadrature is employed herein. This requires that the stresses and strains be evaluated at a selected finite number of stations over the areawise and depthwise region of each element.

Knowing $\{q^*\}_{m+1}$, one can calculate the strain increment $(\Delta\gamma_{ij})_{m+1}$ from time t_m to t_{m+1} at any station in the element from the relation

$$(\Delta\gamma_{ij})_{m+1} = \lfloor D_{ij}\rfloor\{\Delta q\}_{m+1} + \lfloor q\rfloor_{m+1}\{D_{ai}\}\lfloor D_j^a\rfloor\{\Delta q\}_{m+1} - (\Delta\lfloor q_m\rfloor_{+1}\{D_{ai}\}\lfloor D_j^a\rfloor\{\Delta q\}_{m+1})/2 \quad (15)$$

where

$$\{\Delta q\}_{m+1} = \{q\}_{m+1} - \{q\}_m. \quad (15a)$$

With the knowledge of the stresses at time t_m and the strain increments, one can determine the stress increment and the stresses at time t_{m+1} by using the pertinent elastic–plastic stress–strain relations including the yield criterion and flow rule.

2.3 *Evaluation of stresses and plastic strains*

A convenient way to compute the stress increment and/or plastic strain increment at any station (such as Gaussian, for example) in each element at time t_{m+1}, as discussed in [3] will be employed. Also, because the "mechanical sublayer material model"[15, 16] is adopted, the only constitutive relation utilized is that for a homogeneous, initially isotropic, elastic, perfectly-plastic, strain-rate dependent solid; strain hardening is automatically accommodated by this model which includes kinematic hardening and the Bauschinger effect.

It is assumed that all stresses and strains are known at time t_m and that all displacements are known at time t_{m+1}. To find the stresses $(S_j^i)_{m+1}$ at time t_{m+1}, one begins by assuming that the strain increment $(\Delta\gamma_j^i)_{m+1}$ from time t_m to time t_{m+1} is entirely elastic, and a trial (superscript T) value of stress increment is calculated from the following relation for three-dimensional behavior:

$$(\Delta S_j^i)^T = \frac{E}{1+\nu}\left[(\Delta\gamma_j^i)_{m+1} + \frac{\nu}{1-2\nu}(\Delta\gamma_k^k)_{m+1}\,\delta_j^i\right] \quad (16)$$

where E is Young's modulus, v is Poisson's ratio and δ_j^i is the Kronecker delta. Hence, the trial stresses at time t_{m+1} are given by

$$(S_j^i)_{m+1}^T = (S_j^i)_m + (\Delta S_j^i)_{m+1}^T. \tag{17}$$

Then a check is performed by substituting this trial value of the stress into the Mises–Hencky yield function[17, 18], Φ, to determine whether or not the trial stress state lies inside of the yield surface; thus

$$\Phi_{m+1}^T = [(S_j^i)_{m+1}^T (S_i^j)_{m+1}^T - \tfrac{1}{3}(S_k^k S_k^k)_{m+1}^T] - \tfrac{2}{3}\sigma_y^2 \tag{18}$$

where σ_y is the appropriately known uniaxial yield stress of a given mechanical sublayer of the material-behavioral model.

If $\Phi_{m+1}^T < 0$, the trial stress state lies within the elastic domain bounded by the yield surface. Therefore, for this time step there has been no plastic flow and the incremental deformation can be only elastic. Hence, the actual stress $(S_j^i)_{m+1}$ is equal to the trial stress; thus

$$(S_j^i)_{m+1} = (S_j^i)_{m+1}^T \tag{19}$$

and the plastic strain state is

$$(\gamma_j^i)_{m+1}^p = (\gamma_j^i)_m^p. \tag{20}$$

However, if $\Phi_{m+1}^T \geq 0$, the trial stress state lies on or outside of the yield surface (i.e. in the undefined region). Therefore, the trial assumption that the entire strain increment is an elastic-strain increment is not valid. Plastic flow has occurred within this time step and the actual stress state must lie on the yield surface according to the theory of perfect plasticity; then the calculation proceeds as follows. The total strain increment may be decomposed into elastic and plastic components

$$(\Delta\gamma_j^i)_{m+1} = (\Delta\gamma_j^i)_{m+1}^e + (\Delta\gamma_j^i)_{m+1}^p. \tag{21}$$

Since the material is assumed to be incompressible with regard to plasticity and by the flow rule[17, 18], one has

$$(\Delta\gamma_j^i)_{m+1}^p = (\Delta\gamma_j^i)_{m+1}^{Dp} = (S_j^i)_{m+1}^{DT}\lambda \tag{22}$$

where $(\Delta\gamma_j^i)^{Dp}$ is the deviatoric component of the plastic strain increment, and λ is a real nonnegative scalar quantity; also, the deviatoric component of the trial stress $(S_j^i)_{m+1}^{DT}$ which lies between $(S_j^i)_m{}^D$ and $(S_j^i)_{m+1}^D$ is used to approximate the actual deviatoric stress value. Then the stress increment is

$$(\Delta S_j^i)_{m+1} = \frac{E}{1+v}\left[(\Delta\gamma_j^i)_{m+1} + \frac{v}{1-2v}(\Delta\gamma_k^k)_{m+1}\delta_j^i - (S_j^i)_{m+1}^{DT}\lambda\right] \tag{23}$$

and the actual stress at time t_{m+1} is

$$(S_j^i)_{m+1} = (S_j^i)_m + (\Delta S_j^i)_{m+1} = (S_j^i)_{m+1}^T - (S_j^i)_{m+1}^{DT}\bar{\lambda}. \tag{24}$$

The plastic strain at time t_{m+1} is

$$(\gamma_j^i)_{m+1}^p = (\gamma_j^i)_m{}^p + (S_j^i)_{m+1}^{DT}\lambda. \tag{25}$$

The quantity λ and $\bar{\lambda}(\equiv\lambda E/(1+v))$ in equations (24) and (25) can be determined from the fact that $(S_j^i)_{m+1}$ must satisfy the yield condition:

$$\Phi_{m+1} = [(S_j^i)_{m+1}(S_i^j)_{m+1} - \tfrac{1}{3}(S_k^k)_{m+1}^2] - \tfrac{2}{3}\sigma_y^2 = 0. \tag{26}$$

Substituting equation (24) into equation (26) and solving for $\bar{\lambda}$ one obtains the physically valid value

$$\bar{\lambda} = C/(B + \sqrt{B^2 - AC}) \tag{27}$$

where

$$\begin{aligned} A &= (S_j^i)_{m+1}^{DT}(S_i^j)_{m+1}^{DT} - \tfrac{1}{3}(S_k^k S_k^k)_{m+1}^{DT} \\ B &= (S_j^i)_{m+1}^{T}(S_i^j)_{m+1}^{DT} - \tfrac{1}{3}(S_k^k)_{m+1}^{T}(S_k^k)_{m+1}^{DT} \\ C &= \Phi_{m+1}^{T} = (S_j^i)_{m+1}^{T}(S_i^j)_{m+1}^{T} - \tfrac{1}{3}(S_k^k S_k^k)_{m+1}^{T} - \tfrac{2}{3}\sigma_y^2 \end{aligned} \tag{27a}$$

The preceding discussion has pertained to the use of elastic, perfectly-plastic rate-independent material whose yield stress is $\sigma_y \equiv \sigma_0$, the static value. However, if the yield stress is rate dependent, the same procedure applies except that the yield stress σ_y in equations (18) and (26) is the strain-rate-dependent yield stress which is given approximately by[2, 19]:

$$\sigma_y = \sigma_0[1 + |\dot{\varepsilon}/D|^{1/p}] \tag{28}$$

where σ_0 is the static uniaxial yield stress, D and p are material constants, and $\dot{\varepsilon}$ is the uniaxial strain rate. For the three-dimensional problem, it is assumed that $\dot{\varepsilon}$ of equation (28) may be replaced by the second invariant of the deviatoric strain-rate tensor. Thus, this equivalent strain rate is given by

$$\dot{\varepsilon} = \sqrt{(\tfrac{3}{2}[\dot{\gamma}_j^i \dot{\gamma}_i^j - \tfrac{1}{3}(\dot{\gamma}_k^k)^2])} \tag{29}$$

where the strain-rate components $\dot{\gamma}_j^i$ are given by $\dot{\gamma}_j^i = (\Delta\gamma_j^i)/(\Delta t)$.

The discussion spanning equation (16) to equation (29) applies to any given mechanical sublayer of the material model at any spanwise or depthwise Gaussian (or checking) station in the structure. Such a procedure is applied to every mechanical sublayer of the material model at that Gaussian station.

During the operation of this solution process for intensive loading problems, instances of large strain increments can occur which sometimes may lead to an imaginary value of λ. Since the time-step size for that particular instance cannot be economically reduced, a sub-increment procedure to circumvent this difficulty as discussed in [20] can be, and is, used.

3. QUADRILATERAL CYLINDRICAL PANEL ELEMENT

3.1 *Displacement field*

The geometry and nomenclature of a typical quadrilateral cylindrical panel element are shown in Fig. 1. The radius is R. The reference Cartesian coordinate systems are (Y^1, Y^2, Y^3) and (y^1, y^2, y^3). The local cylindrical shell coordinate system is (ξ, η, ζ).

Let the Kirchhoff–Love hypothesis be employed. The displacement field $\bar{u}$, $\bar{v}$, and $\bar{w}$ of the shell may be approximated by the middle surface displacements u, v, and w, and rotations ϕ and ψ as follows:

$$\begin{aligned} \bar{u}(\xi, \eta, \zeta) &= u(\xi, \eta) - \zeta\phi(\xi, \eta) \\ \bar{v}(\xi, \eta, \zeta) &= v(\xi, \eta) - \zeta\psi(\xi, \eta) \\ \bar{w}(\xi, \eta, \zeta) &= w(\xi, \eta) \end{aligned} \tag{30}$$

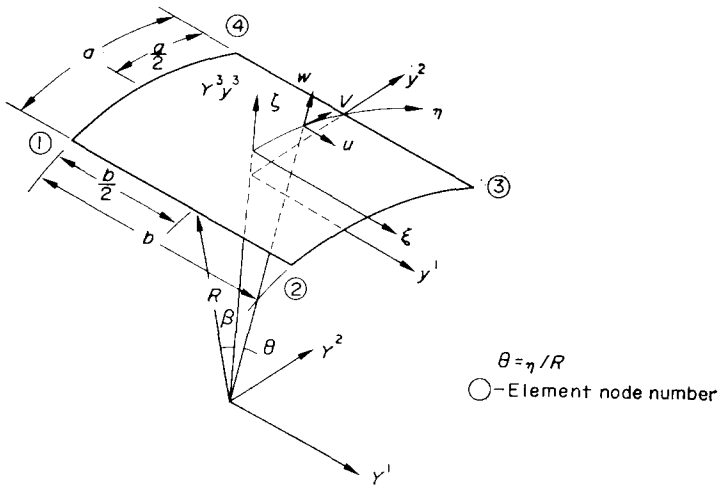

Fig. 1. Quadrilateral cylindrical panel discrete element.

where

$$\phi(\xi, \eta) = \partial w/\partial \xi$$
$$\psi(\xi, \eta) = (\partial w/\partial \eta) - v/R. \tag{30a}$$

The engineering component of the nonvanishing strain distributions may be expressed as

$$\bar{\varepsilon}_{\xi\xi} = \varepsilon_{\xi\xi} - \zeta\kappa_{\xi\xi}$$
$$\bar{\varepsilon}_{\eta\eta} = \varepsilon_{\eta\eta} - \zeta\kappa_{\eta\eta} \tag{31}$$
$$\bar{\varepsilon}_{\xi\eta} = \varepsilon_{\xi\eta} - \zeta\kappa_{\xi\eta}$$

where $\varepsilon_{\xi\xi}$, $\varepsilon_{\eta\eta}$, and $\varepsilon_{\xi\eta}$ are the midsurface inplane strains, and $\kappa_{\xi\xi}$, $\kappa_{\eta\eta}$, and $\kappa_{\xi\eta}$ are the curvature changes. In the formulation of the present problem, the Sanders nonlinear strain–displacement relations are employed which for the cylindrical shell may be written as:

$$\varepsilon_{\xi\xi} = (\partial u/\partial \xi) + (\phi^2 + \psi^2)/2$$
$$\varepsilon_{\eta\eta} = (\partial v/\partial \eta) + (w/R) + (\phi^2 + \psi^2)/2$$
$$\varepsilon_{\xi\eta} = (\partial u/\partial \eta) + (\partial v/\partial \xi) + \phi\psi$$
$$\kappa_{\xi\xi} = \partial\phi/\partial\xi \tag{32}$$
$$\kappa_{\eta\eta} = \partial\psi/\partial\eta$$
$$\kappa_{\xi\eta} = (\partial\phi/\partial\eta) + (\partial\psi/\partial\xi) + \chi/R$$

where

$$\chi = (\partial u/\partial \eta - \partial v/\partial \xi)/2. \tag{32a}$$

The selection of a suitable interpolation function to represent each of these displacements throughout each element is one of the principal concerns in the construction of a finite-element assemblage of the whole structure. For small-deflection, linear-elastic problems,[22] reported a quadrilateral cylindrical-panel element where bicubic-degree polynomials (first order Hermite interpolation in ξ and η) are used to represent both the inplane

displacements u, v, and the out-of-plane displacement, w; 12 degrees of freedom (dof's) at each corner node (denoted, for convenient reference, as C.C.C. or cubic, cubic, cubic element). Reference [23] reports a study of a quadrilateral element with bilinear polynomials for u and v, and bicubic polynomilas for w; 6 dof's per node (termed as L.L.C. or linear, linear, cubic element). It has been concluded[23] that the explicit inclusion of rigid-body displacement modes in the assumed displacement field lead to a much better coarse-mesh solution than if the rigid-body modes were excluded from the assumed displacement functions, despite the fact that incompatibility of the displacements along the circumferential edges is introduced by the explicitly-added rigid-body modes which are expressed in terms of trigonometric functions. Further, it has been found in [10] and [24] for ring examples and in the present study for a cylindrical shell example that the accuracy and convergence behavior of the predictions can be improved further by using an L.C.C. element (or linear, cubic, cubic element); that is, bilinear polynomial for the axial displacement u, and bicubic polynomials for both the circumferential displacement v and the transverse displacement, w, and with the rigid body modes included explicitly. This L.C.C. assumed displacement function can be written as

$$
\begin{aligned}
u &= \alpha_1 + \xi\alpha_2 + \eta\alpha_3 + \xi\eta\alpha_4 - R\sin\theta\alpha_6 + R(\cos\theta - \cos\beta)\alpha_{10} \\
v &= \cos\theta\alpha_5 + \xi\cos\theta\alpha_6 + \eta\alpha_7 + \xi\eta\alpha_8 - \sin\theta\alpha_9 \\
&\quad + \xi\sin\theta\alpha_{10} - R(1 - \cos\theta\cos\beta)\alpha_{11} + \xi^2\alpha_{25} + \eta^2\alpha_{26} \\
&\quad + \xi^2\eta\alpha_{27} + \xi\eta^2\alpha_{28} + \xi^2\eta^2\alpha_{29} + \xi^3\alpha_{30} + \eta^3\alpha_{31} \\
&\quad + \xi^3\eta\alpha_{32} + \xi\eta^3\alpha_{33} + \xi^3\eta^2\alpha_{34} + \xi^2\eta^3\alpha_{35} + \xi^3\eta^3\alpha_{36} \\
w &= \sin\theta\alpha_5 + \xi\sin\theta\alpha_6 + \cos\theta\alpha_9 - \xi\cos\theta\alpha_{10} \\
&\quad + R\sin\theta\cos\beta\alpha_{11} + \xi\eta\alpha_{12} + \xi^2\alpha_{13} + \eta^2\alpha_{14} \\
&\quad + \xi^2\eta\alpha_{15} + \xi\eta^2\alpha_{16} + \xi^2\eta^2\alpha_{17} + \xi^3 a_{18} + \eta^3\alpha_{19} \\
&\quad + \xi^3\eta\alpha_{20} + \xi\eta^3\alpha_{21} + \xi^3\eta^2\alpha_{22} + \xi^2\eta^3\alpha_{23} + \xi^3\eta^3\alpha_{24}
\end{aligned} \tag{33}
$$

where α_1, $\alpha_2 \ldots \alpha_{36}$ are parameters which will be expressed in terms of the generalized nodal displacements. Except for the terms from α_{25} to α_{36}, the field represented by equation (33) is that of the L.L.C. element function of [23].

The generalized nodal displacements which are chosen to characterize the deformation state of the element, are selected such that there are nine degrees of freedom u, v, w, ϕ, ψ, $\partial^2 w/\partial\xi\,\partial\eta$, $\partial v/\partial\xi$, $\partial v/\partial\eta + w/R$, and $\partial^2 v/\partial\xi\,\partial\eta$ at each of the four corner nodes of the element.

For the static linear-elastic pinched cylinder example of Fig. 2, the predictions of the displacement under the load obtained by using the present L.C.C. element and those of [22] and [23] are given in Table 1. Advantage of symmetry is taken by analyzing only one octant of the cylindrical shell. It is seen that the L.C.C. element, 135-dof solution is of the same accuracy as the C.C.C. element or the L.L.C. element 180-dof prediction. Incidentally, Timoshenko's analytical solution[25] tends to be somewhat too stiff, because an inextensional theory is used.

3.2 *Stress–strain relation*

Because of nonlinear material behavior, although the strain variation through the shell thickness, by the Kirchhoff–Love hypothesis, is linear, the variation of stress across the

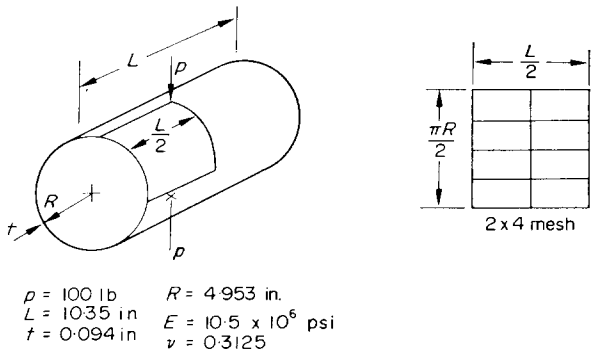

Fig. 2. Pinched cylinder.

thickness may be nonlinear. For computational convenience, the stresses and strains are evaluated at selected Gaussian points across the thickness, and the corresponding weighting factors are used in evaluating the pertinent integrals by Gaussian quadrature. The strain-hardening behavior of the material is accounted for by using the mechanical sublayer material behavior model in which the material at each Gaussian station is treated as consisting of equally-strained sublayers of elastic, perfectly-plastic material with each sublayer having the same elastic modulus but an appropriately different yield stress[15, 16].

The Mises–Hencky yield condition for the plane-stress case is

$$\Phi = \sigma_{\xi\xi}^2 + \sigma_{\eta\eta}^2 - \sigma_{\xi\xi}\sigma_{\eta\eta} + 3\sigma_{\xi\eta}^2 - \sigma_y^2 = 0 \tag{34}$$

where σ_y is the known uniaxial yield stress of a given mechanical sublayer of the material model. This condition establishes a stress boundary such that all possible stress states lie within or on the envelope $\Phi = 0$. In the event that the path between two successive states lies completely within the envelope, the stresses are below the elastic limit; only elastic strains occur. The relation between stress increments and elastic strain increments may be assumed to be linear and to obey Hooke's law:

Table 1. Displacement under the load of the pinched cylinder†

Mesh	Present (L.C.C. element)		Bogner *et al.*[22] (C.C.C. element)		Cantin & Clough[23] (L.L.C. element)		L.L.C. element but without rigid-body modes[23]	
	No. of eqs.	Displ. in.	No. of eqs.	Displ. in.	No. of eqs.	Displ. in.	No. of eqs.	Displ. in.
2 × 2	81	−0·0897	108	−0·0808				
2 × 3	108	−0.1066	144	−0·1036				
2 × 4	135	−0·1106	180	−0·1098				
2 × 5	162	−0·1119			108	−0·0780	108	−0·00266
2 × 7					144	−0·1002	144	−0·00420
2 × 9					180	−0·1073	180	−0·00590
3 × 49					1200	−0·1128	1200	−0·05583

† Timoshenko solution[25] (inextensional theory) = −0.1086 in.

$$\Delta\sigma_{\xi\xi} = \frac{E}{1-\nu^2}(\Delta\bar{\varepsilon}_{\xi\xi} + \nu\Delta\bar{\varepsilon}_{\eta\eta})$$

$$\Delta\sigma_{\eta\eta} = \frac{E}{1-\nu^2}(\nu\Delta\bar{\varepsilon}_{\xi\xi} + \Delta\bar{\varepsilon}_{\eta\eta}) \tag{35}$$

$$\Delta\sigma_{\xi\eta} = \frac{E}{2(1+\nu)}\Delta\bar{\varepsilon}_{\xi\eta}.$$

On the other hand, if all or a portion of the stress path lies on the boundary, plastic strains are possible. The direction of the plastic strain increment vector is established by the plastic flow rule in accordance with the theory of the plastic potential[17, 18]. The flow rule can be expressed as follows:

$$\begin{aligned}\Delta\bar{\varepsilon}_{\xi\xi}{}^{p} &= \lambda(2\sigma_{\xi\xi} - \sigma_{\eta\eta})\\ \Delta\bar{\varepsilon}_{\eta\eta}{}^{p} &= \lambda(2\sigma_{\eta\eta} - \sigma_{\xi\xi})\\ \Delta\bar{\varepsilon}_{\xi\eta}{}^{p} &= \lambda 6\sigma_{\xi\eta}\end{aligned} \tag{36}$$

where the plastic flow parameter, λ, is a non-negative quantity which is determined (i) from the fact that the head of the new stress vector must lie on the yield surface, and (ii) by following the procedure as described in subsection 2.3.

4. NUMERICAL RESULTS AND DISCUSSION

In order to evaluate the accuracy and versatility of the present formulation and solution scheme, the explosively loaded 6061–T6 aluminum alloy cylindrical panel depicted schematically in Figs. 3 and 4 has been analyzed. The present large-deflection elastic–plastic predictions are compared with those from available independent PETROS 2 finite-difference (both spatial and temporal) predictions[3] and with high quality experimental records[26].

The cylindrical panel has the following dimensions: external radius, 3·0 in.; axial length, 12·56 in.; arc span between supports, 120°; and thickness, 0·125 in. All four edges of the panel are "ideally clamped." Over the explosively-loaded portion of the shell, the initial

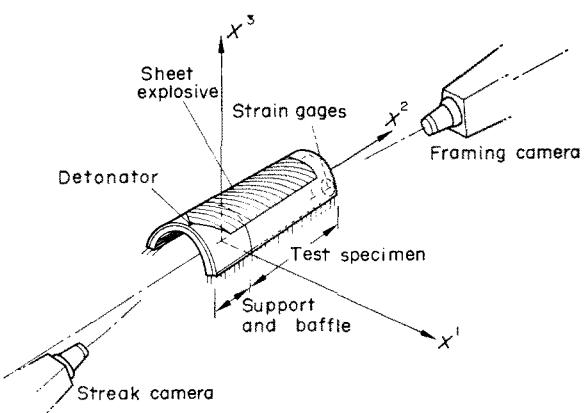

Fig. 3. Experimental arrangement for an explosively-loaded cylindrical panel.

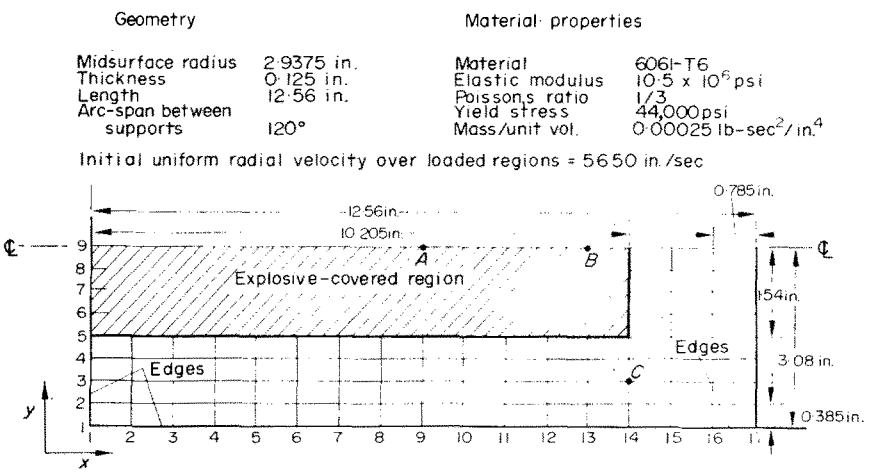

Fig. 4. Grid layout for cylindrical panel experiment.

inward radial velocity is 5650 in/sec; elsewhere the initial velocity is zero. Taking into account symmetry of the explosive loading pattern and geometry, only one half of the cylindrical panel with the symmetry-prescribed-displacement conditions imposed along the crown line is modeled. The geometry of this portion is defined in Fig. 4. Since the 6061–T6 shell material exhibits very little strain hardening, its behavior can be reasonably approximated as being elastic, perfectly-plastic (EL–PP); accordingly, for convenience of legitimate comparison with available past independent predictions of the response of this panel and for economy reasons, EL–PP behavior with $E = 10{\cdot}5 \times 10^6$ psi, $\sigma_0 = 44{,}000$ psi, and $\nu = 1/3$ has been employed in the present predictions and comparisons. However, if desired, one can readily take into account the rather small strain-hardening and strain-rate effects of this material.

Concerning the numerical evaluation of the integrals for determining $\{F_q^{NL}\}$, $\{F_p^{L}\}$ and $\{F_p^{NL}\}$ of equation (11), nine Gaussian stations (3 × 3 product) for carrying out the area integration over each quadrilateral element and 4 depthwise Gaussian points at each areawise Gaussian station are used, since it has been found that this suffices for providing accurate evaluations.

Before predictions of desired accuracy can be obtained, the question of convergence of the solution as the space-mesh size is made finer successively is considered. The peak deflection of point $A(x, y) = (9, 9)$ on the crown line of the cylindrical panel (see Fig. 4) is plotted in Fig. 5 against the smallest side Δy of the mesh. This is chosen as a gross (or global) index of convergence. By using the L.C.C. element, three different mesh sizes: 3, 5, and 7 elements in the circumferential direction are studied; in each case, 8 elements in the longitudinal direction are used. The meshes are denoted, for convenience, as 8 × 3, 8 × 5, and 8 × 7, respectively. It is seen that the convergence of the present solutions is monotonic from below toward the reference value (the experimental result, 1·25 in. is taken as the reference value). Also, it is seen that the L.L.C. element predictions with meshes 8 × 3, 14 × 5, and 10 × 7, tend to be somewhat too stiff to match the experimental value—in comparison with the L.C.C. element coarse-mesh solutions. Shown also in Fig. 5 is the PETROS 2 finite-difference predictions[3] where much finer meshes 12 × 6, 16 × 8, 20 × 10, and 24 × 12 have been used.

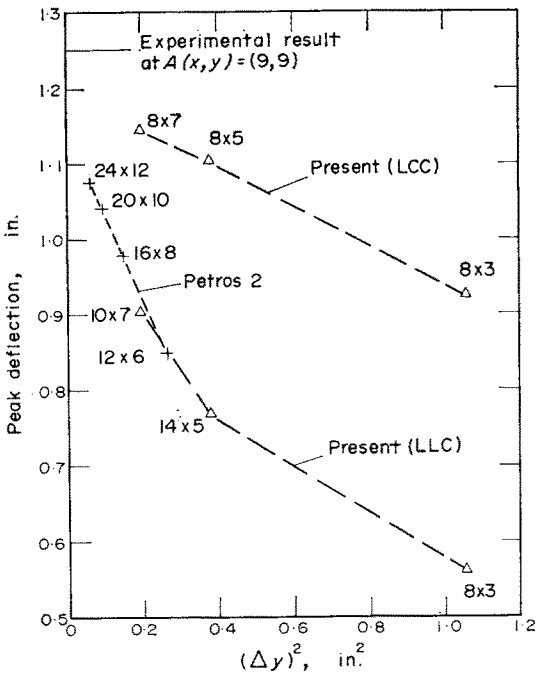

Fig. 5. Convergence of the peak deflection as the mesh size is decreased.

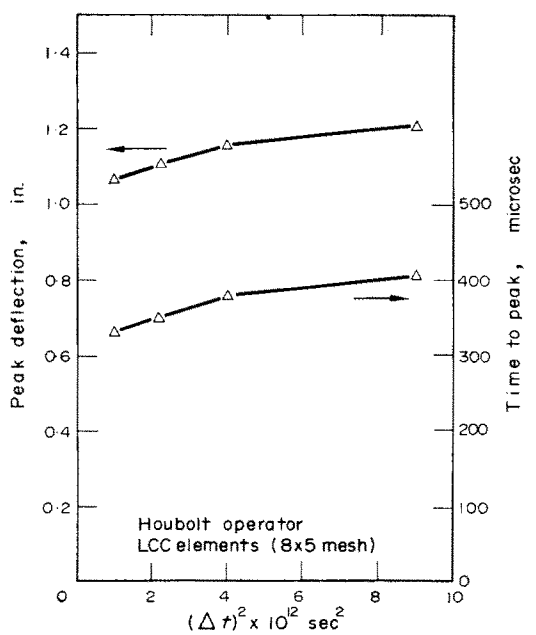

Fig. 6. Effects of the time step size on the peak deflection.

The above finite-element convergence studies were performed by using the Houbolt operator with a time-step size of $\Delta t = 1{\cdot}5$ μsec. However, it perhaps should be noted that since for the present nonlinear dynamic system a reliable and validated criterion by which the proper time-step size can be chosen *a priori* is not readily available, numerical experimentation must be carried out to provide a suitably small Δt to insure both the stability and the convergence of the time-wise integration operator. Illustrated in Fig. 6 are the peak deflection at point A and the time to the peak deflection vs the square of the time-step size; an 8×5 space-mesh of L.C.C. elements is employed.

In order to assess the present predictions, typical comparisons of the deflection responses (as a global index) and the strain responses (as a local-effect index) are made in the following.

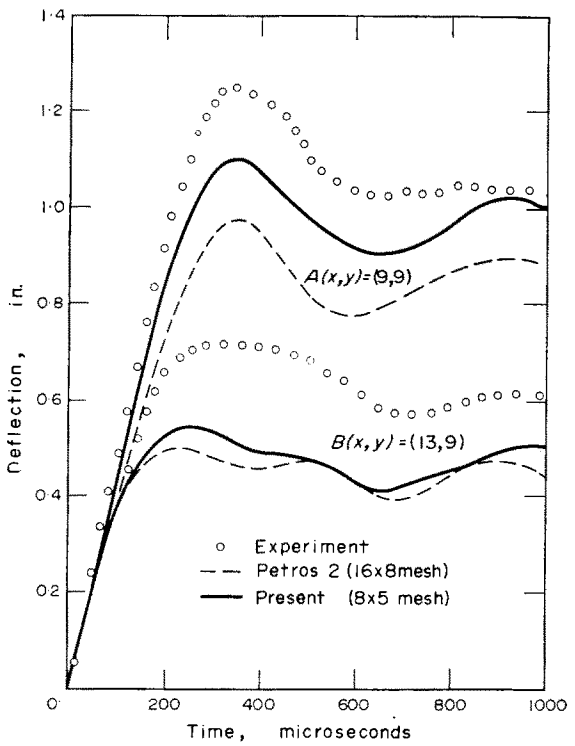

Fig. 7. Comparison of predicted cylindrical panel crown deflection reponse histories with experiment.

Shown in Fig. 7 are the measured and predicted time histories of the mid-surface transverse displacements of two points $A(x, y) = (9, 9)$ and $B(x, y) = (13, 9)$ on the crown line of the cylindrical panel. Calculations which utilize a comparable number of degrees of freedom are selected for presentation here. Accordingly, one half of the cylindrical panel was modeled by an 8×5 mesh of L.C.C. type finite-elements (486 dofs), or by 16×8 finite-difference space meshes with 3 dof's at each space-mesh station (total 459 dof's); the timewise integration operators used are the Houbolt operator with a time-step size of $1{\cdot}5$ μsec and the 3-point central difference operator with a time-step size of $5/3$ μsec, respectively, for the present finite-element (FE) and the PETROS 2 finite-difference (FD) calculations. From this comparison with experimental results, it is seen that the present FE prediction is

somewhat better than the PETROS 2 FD prediction; however, both calculations underpredict the peak deflection. Taking into account the convergence studies shown in Fig. 5, as the mesh size is made finer, a tendency toward a better correlation can be expected. Also, in the calculations, the clamped edges of the panel were treated as being ideally clamped; however, the achievement of an ideally-clamped edge in the experiment may not have been achieved. This reality should be considered in the theoretical–experimental comparisons.

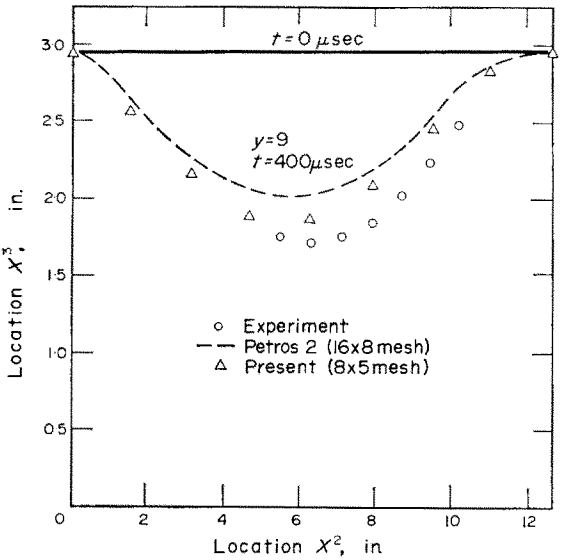

Fig. 8. Comparison of instantaneous cylindrical panel crown deformation profile for predictions and experiment.

Shown versus the experimental result in Fig. 8 are the present FE-predicted and PETROS 2 FD-predicted deformation profiles of the cylindrical panel crown-line (line at circumferential station $y = 9$) at a time of 400 μsec. Another comparison is made in Fig. 9 for the estimates of the final permanent deformation profile of a cross section at an axial station $x = 9$. It was based upon an examination of the time-history behavior of the predicted responses that the profile at $t = 1000$ μsec would represent a reasonably good estimate of the permanent deformation. Figures 8 and 9 show that both the present predictions and the PETROS 2 predictions are in reasonably close agreement with experiment, with the finite-element prediction being somewhat better.

The dynamic strain responses provide a local and more sensitive quantity for examination. Figure 10 shows the time history of the inner surface circumferential strain at point $C(x, y) = (14, 3)$. The PETROS 2, 16×8 space-mesh predicted strain responses (plotted in Fig. 10a) is largely one of tension as compared with compression which was measured during about the first 600 μsec. However, as space-mesh size is made finer, improvement in agreement is observed, such as illustrated by the 32×16 space-mesh prediction and the array B mesh prediction[3]. The meshing used in array B was the uniform 16×8 mesh but modified to be finer near each clamped edges by the addition of 4 evenly-interspersed coordinate curves; a 24×12 nonuniform space-mesh resulted. On the other hand, the present finite-element 8×5 mesh prediction is shown in Fig. 10(b); the strains at point C within the finite element were calculated from the strain–displacement relations, equation

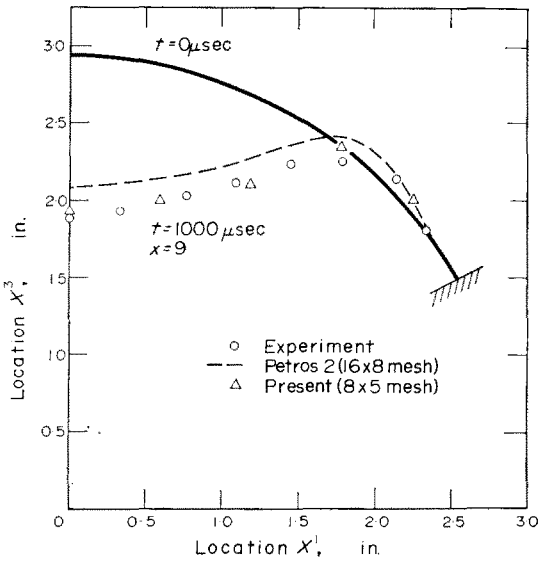

Fig. 9. Estimates of final deflection of a cross section of the cylindrical panel versus experiment.

(32), by taking the derivatives of the assumed displacement function. By noting the coarseness of the 8×5 mesh employed, the agreement with experiment is considered to be excellent.

Based upon the studies cited here and in [3] and [7], it appears that in order to obtain comparable prediction accuracy, both the storage requirements and the CPU computer time for the FE method vs the FD method are comparable. A similar conclusion is reported in [10] for two-dimensional (beam and ring) structural transient response problems involving large deflections and elastic–plastic behavior.

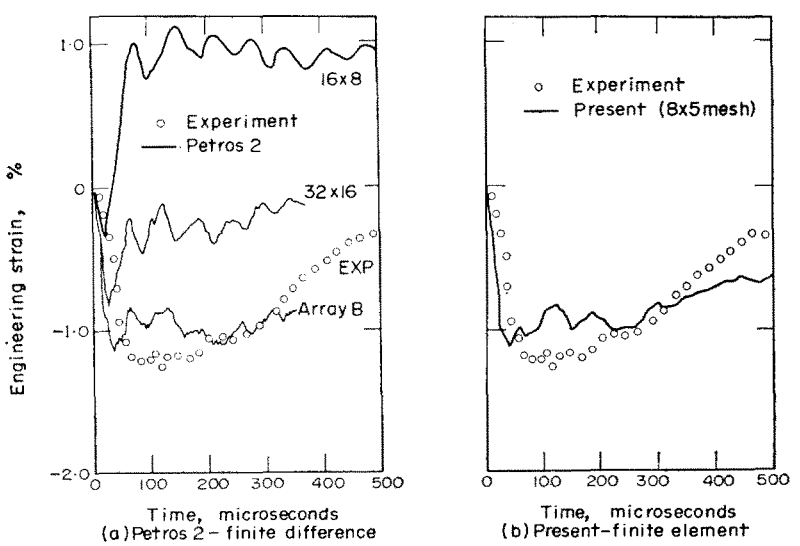

Fig. 10. Comparisons of inner-surface circumferential strains at cylindrical panel station (14, 3).

5. SUMMARY REMARKS

The finite-element solution procedure as described herein has been shown to provide another effective method for treating the large deflection transient responses of a cylindrical shell including elastic–plastic material behavior. The method is capable of providing accurate predictions, especially of the strain, with rather coarse meshes compared with those needed for comparable accuracy by the finite-difference method. A quadrilateral cylindrical panel element is employed. The assumed displacement fields are represented by a bilinear polynomial expression for the axial displacement u, and bicubic polynomials for both the circumferential v and the transverse w displacements, with the rigid-body modes taken into account explicity.

Extensions of the present formulation to complex structures such as stiffened shells and/or structures with cutouts, branches, etc. will be of interest and are in progress.

REFERENCES

1. E. A. Witmer, H. A. Balmer, J. W. Leech and T. H. H. Pian, Large dynamic deformations of beams, rings, plates and shells, *AIAA J.* **1**, 1848–1857 (1963).
2. J. W. Leech, E. A. Witmer and T. H. H. Pian, Numerical calculation technique for large elastic–plastic transient deformations of thin shells, *AIAA J.* **6**, 2352–2359 (1968).
3. L. Morino, J. W. Leech and E. A. Witmer, PETROS 2: A new finite-difference method and program for the calculation of large elastic–plastic dynamically-induced deformations of general thin shells, *J. appl. Mech.* **38**, 423–436 (1971).
4. R. D. Krieg and T. A. Duffey, UNIVALVE II: A code to calculate the large deflection dynamic responses of beams, rings, plates and cylinders. Sandia Laboratories, CR-PR-68-303. Albuquerque, New Mexico (1968).
5. N. J. Huffington, Jr., *Large Deflection Elastoplastic Response of Shell Structures.* U.S. Army Ballistic Research Laboratories, Report No. 1515, November (1970).
6. P. Underwood, *User's Guide to the SHORE Code.* Lockheed Missles and Space Co., Palo Alto, California. Report LMSC-D244589 (1973).
7. S. Atluri, E. A. Witmer, J. W. Leech and L. Morino, *PETROS 3: A Finite-Difference Method and Program for the Calculation of Large Elastic–Plastic Dynamically-Induced Deformations of Multilayer Variable-Thickness Shells.* Massachusetts Institute of Technology, ASRL TR 152-2 (BRL CR 60) Cambridge, Massachusetts (1971).
8. S. D. Pirotin, L. Morino, E. A. Witmer and J. W. Leech, *Finite-Difference Analysis for Predicting Large Elastic–Plastic Transient Deformations of Variable-Thickness Soft-Bonded Thin Shells.* Massachusetts Institute of Technology, ASRL TR 152-3 (1972).
9. R. W-H. Wu and E. A. Witmer, Finite-element analysis of large elastic–plastic transient deformations of simple structures, *AIAA J.* **9**, 1719–1724 (1971).
10. R. W-H. Wu and E. A. Witmer, *Finite-Element Analysis of Large Transient Elastic–Plastic Deformations of Simple Structures with Application to the Engine Rotor Fragment Containment/Deflection Problem.* Massachusetts Institute of Technology, ASRL TR 154-4 (also available as NASA CR-120886), Cambridge, Massachusetts (1972).
11. J. A. Stricklin, W. E. Haisler, W. A. Von Riesemann, R. D. Leick, B. Hunsaker and K. E. Saczalski, *Large Deflection Elastic–Plastic Dynamic Response of Stiffened Shells of Revolution.* TEES-RPT-72-25 and SLA-73-0128. Aerospace Engineering Dept., Texas A & M Univ., College Station, Texas (1972).
12. J. F. McNamara and P. V. Marcal, Incremental Stiffness Method for Finite Element Analysis of Nonlinear Dynamic Problems, Paper presented at *International Symposium of Numerical and Computer Methods in Structural Mechanics*, Sept. 1971, Urbana, Illinois.
13. H. D. Hibbitt, P. V. Marcal and J. R. Rice, A Finite Element Formulation for Problems of Large Strain and Large Displacement. Rept. N00014-0007/2, Div. of Engineering, Brown University, Providence, R.I.
14. J. C. Houbolt, A recurrence matrix solution for the dynamic responses of elastic aircraft, *J. Aero. Sci.* **17**, 540–550 (1950).
15. W. Prager and P. G. Hodge, Jr. *Theory of Perfectly Plastic Solids.* Dover (1951).
16. G. N. White, Jr., *Application of the Theory of Perfectly Plastic Solids to Stress Analysis of Strain Hardening Solid.* Graduate Div. of Applied Maths., Brown University, Tech. Report 51, August 1950, Providence, R.I.

17. R. Hill, *Mathematical Theory of Plasticity*. Clarendon Press (1950).
18. A. Mendelson, *Plasticity: Theory and Application*. Macmillan (1968).
19. T. C. T. Ting, *The Plastic Deformation of a Cantilever Beam with Strain Rate Sensitivity under Impulsive Loading*. Brown University, TR 70, ONR Contract 562(10), Providence, R.I. July (1961).
20. N. J. Huffington, Jr., *Numerical Analysis of Elastoplastic Stress*, U.S. Army Ballistic Research Laboratory, Memorandum Report No. 2006, Aberdeen Proving Ground, Maryland. Sept. 1969.
21. J. L. Sanders, Jr., Nonlinear theories for thin shells, *Q. appl. Math.* **21**, 21–36 (1963).
22. F. K. Bogner, R. L. Fox and L. A. Schmit, A cylindrical shell discrete element, *AIAA J.* **5**, 745–750 (1967).
23. G. Cantin and R. W. Clough, A curved, cylindrical shell discrete element, *AIAA J.* **6**, 1057–1062 (1968).
24. R. H. Coco, *Stiffness Matrix for Curved–Tapered and Straight–Tapered Shell Stiffeners*, SAMSO TR 69-135 (also MIT ASRL TR 146-6), Cambridge, Massachusetts. March (1969).
25. S. Timoshenko and S. Woinowsky-Krieger, *Theory of Plates and Shells*. McGraw-Hill (1959).
26. E. W. Clark, F. H. Schmitt and I. P. Juriaco, *Plastic Deformation of Structures*. III—*Large Plastic Deformation of Clamped Cylindrical Panels*, FDL-TDR-64864. Picatinny-Arsenal, Dover, N.J. March (1968).

Резюме — Методы анализа финитных элементов применяются для проблемы большого отклонения эластично-пластичной динамической характеристики цилиндрических кожухов при переходной нагрузке. С цель идеализирования структуры цилиндрического кожуха, применяется специальное предположение четырехугольного смещения финитных элементов цилиндрической панели. Формулировка основывается на принципе возможных перемещений и на принципе д'Аламбера. Для решения получившихся уравнений по времени применяется процедура непосредственного численного интегрирования. Предсказанная настоящим динамическая характеристика взрывчато нагруженной цилиндрической панели сравнивается с другими независимыми предсказаниями и с экспериментально вымеренной динамической характеристикой, нашли, что результаты совпали.